Neurobiology of Disease 227 (2026) 107503

Contents lists available at ScienceDirect

Neurobiology of Disease

journal homepage: www.elsevier.com/locate/ynbdi

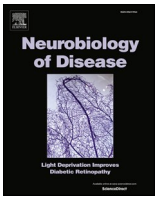

Synaptophysin density underestimates synapse counts in the human brain – An anatomical study on synaptoporin protein expression

Sarah Woelfle [a,b,*], Michael Schön [a], Maria T. Pedro [c], Jan Wagner [d], Ehab Shiban [e], Bujung Hong [e], Yuriy Tsoy [e], Tobias M. Boeckers [a,b,f,*]

[a] Institute for Anatomy and Cell Biology, Ulm University, Albert-Einstein-Allee 11, 89081 Ulm, Germany
[b] Neuroscience Center Ulm (NCU), 89081 Ulm, Germany
[c] Department of Neurosurgery, Ulm University, campus Günzburg, Lindenallee 2, 89312 Günzburg, Germany
[d] Epilepsy Center Ulm, Department of Neurology, University of Ulm Medical Center, 89081 Ulm, Germany
[e] Department of Neurosurgery, Medical University Lausitz – Carl Thiem, Thiemstr. 111, 03048 Cottbus, Germany
[f] Deutsches Zentrum für Neurodegenerative Erkrankungen, DZNE, Ulm site, 89081 Ulm, Germany

ARTICLE INFO

Keywords:
Synaptoporin
Synaptophysin
Human *post mortem* tissue
Immunofluorescence
Synaptome

ABSTRACT

Synaptoporin (SPO; synaptophysin II) has classically been described as a presynaptic vesicle protein enriched in the hippocampal mossy fiber pathway, distinguishing it from the ubiquitously expressed synaptophysin I (SYP). However, its distribution and synapse-type specificity in the human brain have not been studied yet. Here, we comprehensively mapped SPO protein expression across multiple human brain regions using immunofluorescence staining of *post mortem* tissue and biochemical analysis of brain lysates. We identified high SPO protein expression in the hippocampus, cerebral cortex, and dorsal horn of the spinal cord; moderate expression in the cerebellum and amygdala; and low levels in the putamen. The analyzed brainstem regions and the thalamus were devoid of SPO. Notably, SPO was present in distinct components of the human auditory pathway, mirroring rodent patterns. Colocalization analyses revealed largely separate distributions of SPO and SYP, challenging the concept of SYP as 'pan-synaptic' marker. In the cerebral cortex, a region with pronounced SPO expression, SYP-based synapse quantification underestimated total synapse numbers by up to 35%, a result replicated across independent brain tissue sources. SPO puncta were associated with both excitatory and inhibitory synaptic markers, reflecting the highly heterogeneous human synaptome. Collectively, these findings demonstrate that SYP-only assays overlook a substantial subset of synapses and they highlight the combinatorial complexity of vesicle protein expression in the human brain. This work establishes SPO as a critical determinant of synaptic diversity and can serve as reference to identify vulnerable synaptic subtypes in neurodegenerative diseases.

1. Introduction

Synaptophysin II, better known as synaptoporin (SPO), was identified in 1990 (Knaus et al., 1990) and shares some major biochemical properties with synaptophysin I (SYP): both are N-glycosylated proteins with four transmembrane domains that are located within the presynaptic vesicle membrane while the N- and C-terminus are directed towards the cytoplasm (Fykse et al., 1993; Knaus et al., 1990; Leube et al., 1987). In humans, SYP and SPO have similar molecular weights but only 53% amino acids identity (mainly due to C-terminus). The genes encoding SYP and SPO are located on the X chromosome and on chromosome 3, respectively. A major difference between the two proteins is their expression pattern in the brain: In contrast to the 'pan-synaptic' marker SYP (Fykse et al., 1993; Jahn et al., 1985; Wiedenmann and Franke, 1985), SPO is mainly known as mossy-fiber enriched protein in the hippocampus (Fykse et al., 1993). However, already initial studies pointed towards a role of SPO beyond the hippocampus and detected considerable mRNA levels in the rat cerebral cortex, cerebellum, olfactory bulb, striatum, epithalamus, superior colliculus, and the dorsal horn of the spinal cord and weaker levels in the hypothalamus, inferior colliculus, and amygdala (Knaus et al., 1990; Marqueze-Pouey et al., 1991). Via immunostaining, SPO was detected in the rodent hippocampus (also beyond CA3), cerebral cortex, cerebellum, striatum, olfactory bulb (Bergmann et al., 1993; Fykse et al., 1993; Grabs et al., 1994;

* Corresponding authors at: Institute for Anatomy and Cell Biology, Ulm University, Albert-Einstein-Allee 11, 89081 Ulm, Germany.
E-mail addresses: sarah.woelfle@uni-ulm.de (S. Woelfle), tobias.boeckers@uni-ulm.de (T.M. Boeckers).

https://doi.org/10.1016/j.nbd.2026.107503
Received 16 April 2026; Received in revised form 20 June 2026; Accepted 22 June 2026
Available online 23 June 2026

Ovtscharoff et al., 1993; Singec et al., 2002), the dorsal horn of the spinal cord (Chung et al., 2019), dorsal root ganglia (Sun et al., 2006), and recently also in regions within the auditory system (Reuss et al., 2023).

Neurodegenerative diseases go along with massive synaptic loss, e.g., in the hippocampus (e.g., (Scheff et al., 2006)) or the cerebral cortex (e.g., (DeKosky and Scheff, 1990)). Apart from first *in vivo* studies which applied PET tracers to measure synapse density (e.g., SV2A tracers (Finnema et al., 2016)), the dynamics and selectivity of synapse loss can only be traced using properly characterized *post mortem* human tissue. To preserve the three-dimensional (3D) aspect and to specifically navigate the analysis to subregions that are known to be more prone to synapse loss (e.g., cortical layer III in Alzheimer's disease (Scheff et al., 1990)), immunostaining is the method of choice. Presynaptic SYP is a popular target since it is expressed at most synapses (Fykse et al., 1993; Jahn et al., 1985; Wiedenmann and Franke, 1985) and it was found to be stable also after longer *post mortem* intervals (Siew et al., 2004). On the contrary, there is growing evidence for a large diversity of human synapse subtypes (recently reviewed in (van Oostrum and Schuman, 2025)), making it more difficult to use one single marker protein. For instance, the presynaptic protein SV2A has been proposed as suitable 'pan-synaptic' marker; however, its expression is restricted to synaptic subpopulations in the human brain (Wong et al., 2025). Such results, in turn, are highly relevant to guide the development of novel tracers or targets tested in clinical studies (see above).

Only little is known about SPO expression in the human brain. In a previous study that focused on the hippocampus, we were able to show that SPO is expressed in nearly all hippocampal layers at excitatory, and most likely also at inhibitory synapses (Woelfle and Boeckers, 2021). The aim of this study was to analyze SPO protein expression in central human brain regions. In addition, the conservation of SPO expression in the auditory system was analyzed. Importantly, in light of the findings from rodent tissue, co-staining of SYP and SPO was performed to assess whether SPO is exclusively expressed at SYP-positive synapses or whether total synapse counts are underestimated when applying SYP as 'pan-synaptic' marker. To this end, human cortical tissue from four different sources (i.e., different fixation techniques, Table 1) was analyzed.

2. Results

2.1. Enrichment of synaptoporin in human hippocampus lysates

To gain a first general overview on the expression of SPO in the human brain, protein expression was analyzed in tissue lysates (Fig. 1a, upper row and Fig. 1b, left). As expected, SPO was enriched in the hippocampus (HC), but considerable levels were also detected in the cerebral cortex (CTX) and amygdala (AMY). Weak SPO levels were measured in the entire diencephalon and the cerebellum (CB). Among the analyzed regions, no SPO was detected in the thalamus (THA) and the brainstem (medulla oblongata and pons). In contrast, SYP was present in comparable levels in the AMY, HC, and the CTX (Fig. 1a, lower row and Fig. 1b, right). In the diencephalon, expression levels were around half of the cortical levels. In the THA in particular and in the brainstem regions, SYP expression was clearly lower than in the CTX (~20%). Only a faint SYP signal was obtained for the CB.

2.2. Synaptoporin expression in central human brain regions

Immunofluorescence (IF)-based analysis of human *post mortem* brain sections from $n = 3$ body donors was performed to confirm western blot findings and to screen additional brain regions (Table 2 and Nissl staining in Fig. S1) for SPO expression. To analyze the number of synapses that express SPO or SYP, the density of IF-positive 3D structures – most likely synapses – was determined in the neuropil: Using Imaris software, these IF-positive structures were transformed into 3D surfaces, whose number and sum intensity was exported and summarized as explained in detail in the "Methods" section. The sum intensity of all detected puncta can be interpreted as a measure for the protein expression level. Since this method does not count single proteins, the sum intensity is referred to as relative expression level.

SPO puncta were enriched in *cornu Ammonis* 3 (CA3) of the HC and lamina I of the dorsal horn of the cervical spinal cord (SC DH) (Fig. 1c, 2 and 10). High puncta densities were obtained in layer V of the CTX (Fig. 1c, 1); in the AMY and the CB (Fig. 1c, 3 and 8), only half the number of SPO puncta was found (Fig. 1d). The putamen (PUT) showed a low density in comparison to the CTX (~20%, Fig. 1c, 4) and SPO puncta were virtually absent from the THA, brainstem (pons, inferior olive, IO), and lamina IX of the ventral horn of the spinal cord (SC VH) (Fig. 1c, 5–7 and 9). Notably, IF-based analysis is only cross-sectional and a negative result does not exclude a possible expression in a sublayer/nucleus that was not subject to the present analysis. However, the western blots from brain lysates had shown the absence of SPO in the entire THA, pons, and medulla oblongata. As seen, e.g., for the CB, the SPO antibody sometimes stained nuclei. This occurred case-dependent and was not observed in the tissue resectates or in mouse sections (data not shown). Since the analysis was performed in regions of interest within the neuropil, the nuclear signals are not reflected by the graphs. In addition to the density, the sum intensity of the detected puncta was analyzed which can be interpreted as relative protein expression level (Fig. 1e). In the HC, the expression is three times higher as in the CTX. In contrast, the difference in puncta density was less pronounced (~1.3 times higher). In the AMY, PUT, and SC DH, the normalized puncta densities were reflected by the sum intensities. The CB had a moderate number of SPO-positive puncta with in summary very low SPO levels.

To determine the colocalization of SPO and SYP, SYP was always co-stained (Fig. 1f). In a first step, SYP puncta density (Fig. S2a) and SYP sum intensity (Fig. S2b) were analyzed individually. In the CB and SC DH, puncta densities were slightly higher than in the CTX. In the HC, THA, and IO, SYP puncta density was between 50 and 72% of cortical

Table 1
Demographics of the $n = 8$ cases.

Case ID	Age (yrs)	Sex	Tissue	NFT stage	Aβ phase	PD stage	PMI (hours)	Fixation year	Cause of death
#1	64	M	Table 2	II	3	0	72	2021	Septic shock
#2	83	M	Table 2	II	1	0	48	2021	Food refusal
#3	86	M	Table 2	II	4	0	72	2022	Cardiac/ pulmonal decompensation
#4	71	M	SN	I	5	0	120	2021	Cardiogenic shock
#5	61	F	Cerebral cortex	N.a.	N.a.	N.a.	4–6	N.a.	N.a.
#6	21[a]	F	Temporal pole	–	–	–	Fixation delay ~45 min	2019	–
#7	74[a]	F	Frontal lobe	N.a.	N.a.	N.a.	Immediate fixation	2025	–
#8	43[a]	F	Frontal lobe	N.a.	N.a.	N.a.	Immediate fixation	2026	–

Yrs years, F female, M male, NFT neurofibrillary tangle, Aβ amyloid-β, PD Parkinson's disease, PMI *post mortem* interval, SN substantia nigra, N.a. not available.
[a] At the time point of surgery.

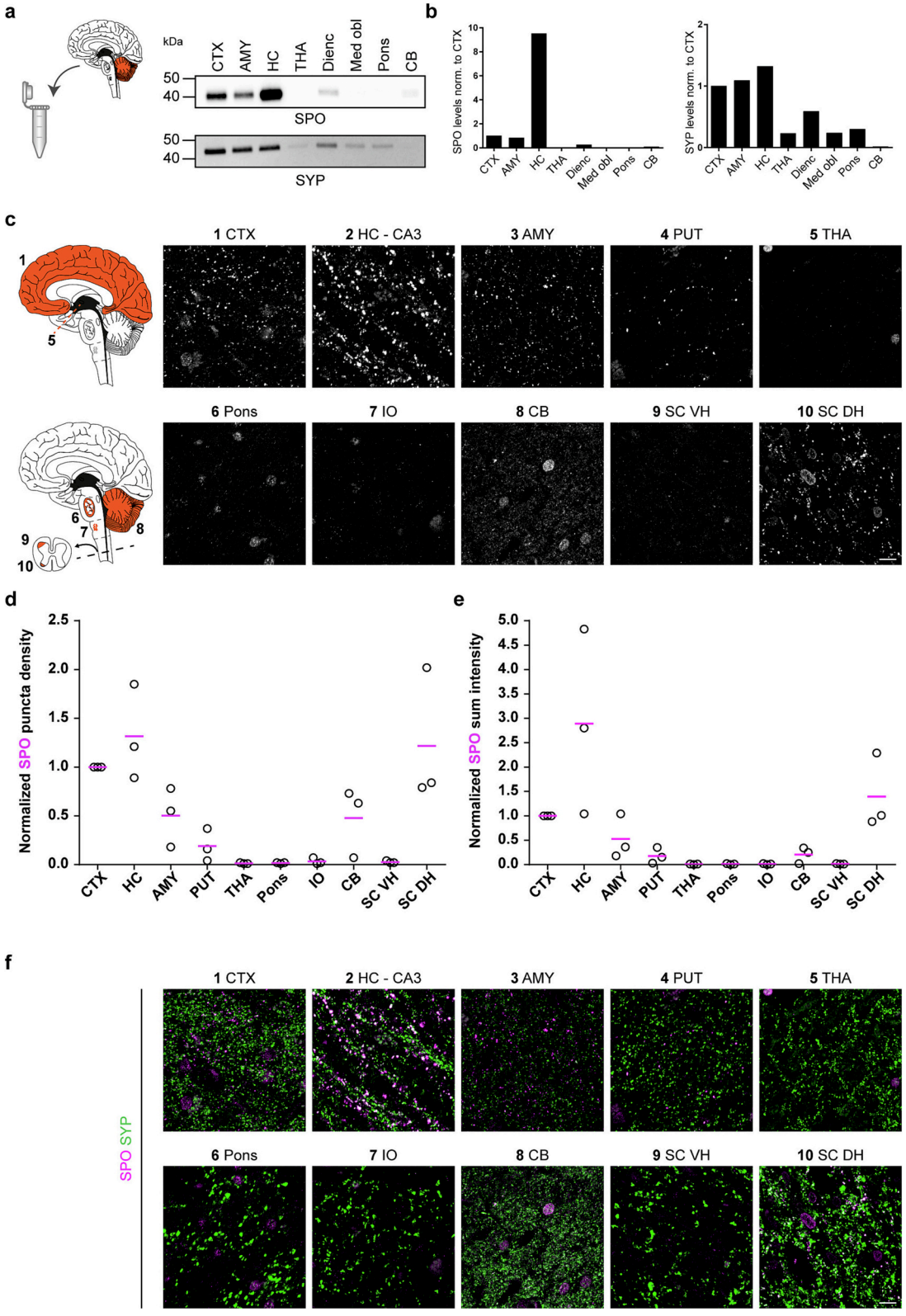

Fig. 1. SPO is enriched in the human hippocampus and strongly expressed in cortex and the dorsal horn of the spinal cord. (a) Western blots were performed to determine SPO and SYP levels in commercially available human brain lysates. kDa = kilodalton, CTX = cortex, AMY = amygdala, HC = hippocampus, THA = thalamus, Dienc = diencephalon, Med obl = medulla oblongata, CB = cerebellum (b) Two technical replicates of the blot in panel (a) were analyzed and band intensities were normalized (norm.) to the levels in the cortex (CTX). (c) Representative images from all immunostained brain regions, ID #1. For details on acquired layers, see Table 2. Images represent maximum intensity projections (MIPs, z = 1.98 µm) of raw data. For all regions, image acquisition and contrast adjustment was performed with identical parameters. Scale bar: 10 µm. Brain schemes were adjusted from (Woelfle et al., 2023b). (d) SPO puncta density from three images per brain region was normalized to the CTX. The results for $n = 3$ individuals (ID #1–3) and their mean are plotted. (e) Normalized sum intensities of the surfaces underlying Fig. 1d. (f) The images from panel (c) are shown as overlay of SPO and SYP staining. Scale bar: 10 µm.

Table 2
Overview on analyzed brain regions.

Brain region	Analyzed subregion/layer	Abbreviation
Cerebral cortex	Superior frontal gyrus, layer V	CTX
Hippocampus	CA3, *stratum pyramidale*	HC – CA3
Amygdala	Lateral (ID #2) and basolateral nucleus	AMY
Putamen	–	PUT
Thalamus	Ventral nuclei	THA
Pons	Pontine nuclei	Pons
Inferior olive	Principal subnucleus	IO
Cerebellum	Cerebrocerebellum, molecular layer	CB
Spinal cord, cervical (~2 cm below pyramids)	Ventral horn, lamina IX	SC VH
	Dorsal horn, lamina I	SC DH
Cochlear nuclear complex		CNC
Superior olivary complex	Around the medial superior olivary nucleus; difficult to distinguish exact borders	SOC
Inferior colliculus	External cortex	IC
Medial geniculate body	Medial subdivision	MGB

levels. In the AMY, PUT, pons, and the SC VH, SYP puncta densities were between 0 and 40% of cortical levels. For the interpretation of especially the brainstem values, it has to be considered that the IF analysis was always performed in synapse-rich areas (see Table 2) in contrast to the lysates which include the large amount of white matter from these regions. The relative SYP expression in the IO, the SC VH, and especially the SC DH (factor of ~3.4) was higher than in the CTX. Hence, in the IO and SC VH, the high SYP protein levels were distributed at a moderate or even low number of SYP-positive synapses. On the contrary, in the CB, similar to SPO, SYP-positive synapses were comparable to the CTX with respect to numbers but had only moderate SYP expression levels. For the remaining regions, the normalized puncta densities were reflected by the sum intensities. In summary, in line with its role as 'pan-synaptic' marker, clear SYP signals were obtained in all analyzed regions. In contrast, SPO was expressed in only a fraction of the analyzed regions (CTX, HC, AMY, PUT, CB, and SC DH).

2.3. Synaptoporin expression in areas within the auditory system

Auditory input reaching the cochlea (site of 1st neuron) is forwarded to the cochlear nuclear complex (CNC, 2nd neuron). From there, the information passes through the inferior colliculus (IC, 3rd neuron in central nucleus), the medial geniculate body (MGB, 4th neuron in dorsal nucleus), and finally reaches the transverse temporal gyri (5th neuron) in the cerebral cortex (= primary auditory cortex). As part of the indirect auditory pathway, the superior olivary complex (SOC) is interconnected after the second neuron. In a recent study in mice, SPO protein expression was observed in particular nuclei within the auditory system (Reuss et al., 2023). We analyzed human SPO expression in all stations of the auditory pathway except for the temporal cortex (Fig. S3a) and focused on the nuclei with moderate to high SPO expression in mice. The aim

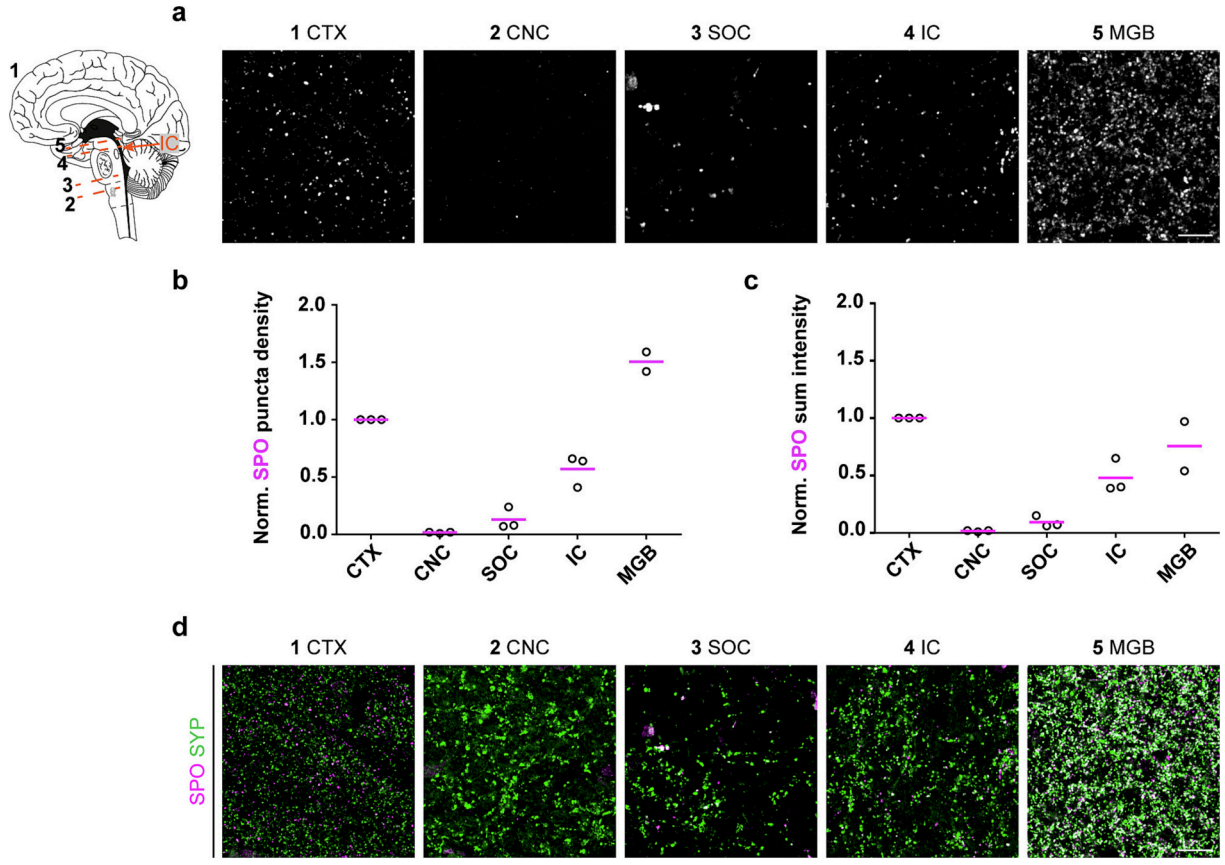

Fig. 2. SPO is selectively expressed in subregions of the auditory system. (a) The scheme on the left (adjusted from (Woelfle et al., 2023b)) shows the approximate cutting levels to cover all stations of the auditory system. SPO immunostaining in the regions shown in Fig. S3a, for details on acquired layers, see Table 2. Images represent maximum intensity projections (MIPs, z = 2 µm) of raw data. For all regions, image acquisition and contrast adjustment was performed with identical parameters. Scale bar: 10 µm. (b) SPO puncta density from three images per brain region was normalized (norm.) to the CTX. The results for n = 3 individuals (ID #1–3) and their mean are plotted. MGB was not available from case ID #2. (c) Normalized sum intensities of the surfaces underlying Fig. 2b. (d) The images from panel (a) are shown as overlay of SPO and SYP staining. Scale bar: 10 µm.

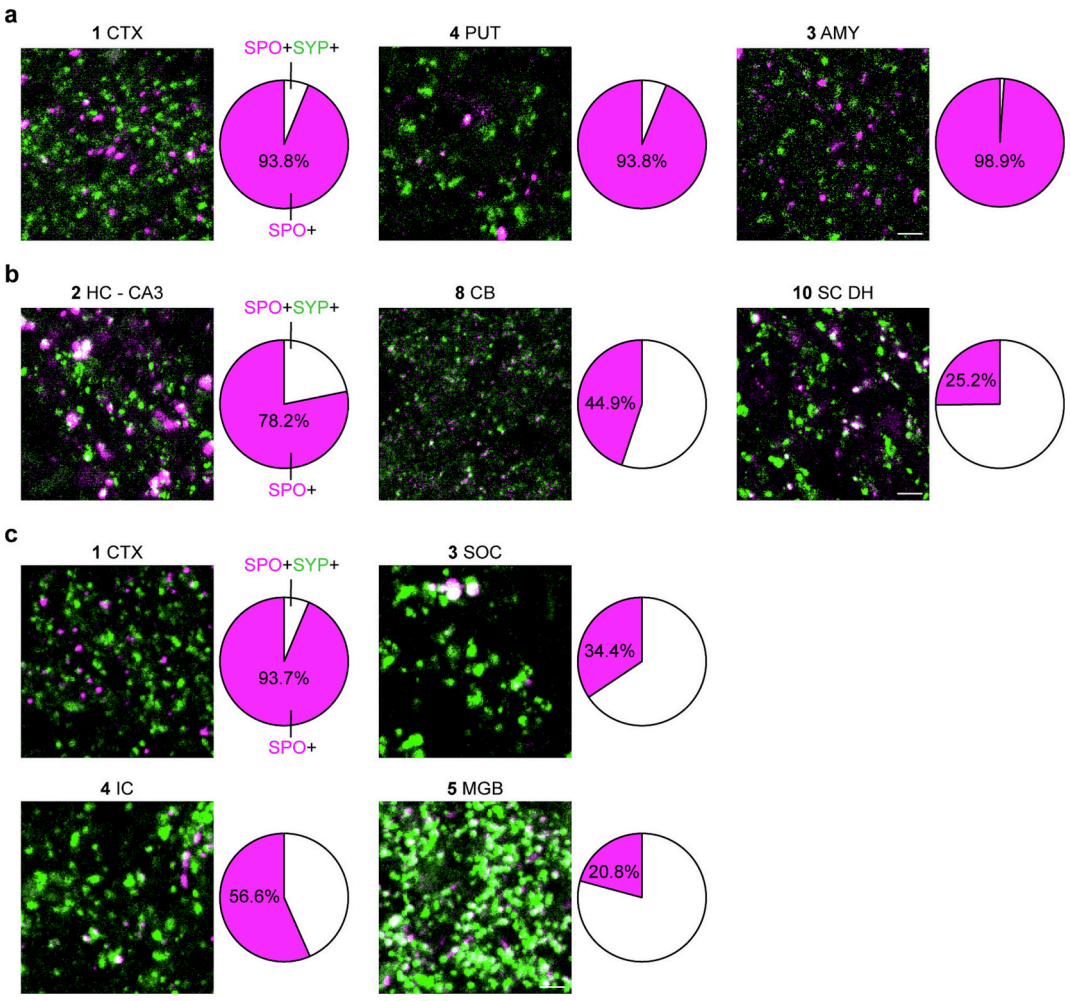

Fig. 3. The majority of SPO surfaces does not colocalize with SYP in most of the regions. (a)-(b) Colocalization of SPO and SYP was analyzed in the images from Fig. 1 and is represented as pie chart (magenta = SPO+/SYP- surfaces, white = SPO+/SYP+ surfaces). The percentages represent the mean of ID #1–3. Scale bars: 3 µm. (c) In the same manner as in panel (a), colocalization data from the regions shown in Fig. 2 are represented. Images represent MIPs of raw data. Scale bar: 3 µm. For this figure, images were individually contrast adjusted to clearly visualize signal overlap. (For interpretation of the references to colour in this figure legend, the reader is referred to the web version of this article.)

was to check conservation of protein expression and to specifically expand protein expression analysis in the human brain. To relate the data to Fig. 1, puncta densities and sum intensities were normalized to the CTX. In the MGB (medial subdivision, Fig. 2a, 5), SPO puncta density was 1.5 times higher than in the CTX (Fig. 2b) but the relative SPO protein expression was lower (Fig. 2c, ~70% of the CTX). Moderate and low densities were found in the IC (external nucleus/cortex; see (Mansour et al., 2019; Sitek et al., 2022), in humans also referred to as lateral zone (Casseday et al., 2005; Tardif et al., 2003) or lateral nucleus (cortex) (Pal et al., 2019)) (Fig. 2a, 4) and the SOC (acquisition around the medial superior olivary nucleus; see also (Lavezzi and Matturri, 2012)) (Fig. 2a, 3), respectively. This was reflected by the relative SPO expression level, i.e., the sum intensity (Fig. 2c). SPO was virtually absent from the CNC (Fig. 2a, 2). On the contrary, SYP was strongly expressed in all analyzed regions (Fig. 2d). Only for the MGB, the puncta density was higher than in the CTX. In the CNC, SOC, and IC, the puncta density measured 50–70% of the cortical density (Fig. S3b). The relative SYP expression in the CNC, SOC, and IC was up to almost twice as high as in the CTX (Fig. S3c). The MGB showed ~4.7 times higher SYP expression compared to the CTX. For comparison of RNA and protein expression levels, the RNA data from 'The Human Protein Atlas' (HPA)[1] were plotted in Fig. S3d.

2.4. *Absence of synaptophysin at the majority of synaptoporin-positive synapses*

Finally, in all analyzed brain regions, the detected SPO- and SYP-positive puncta were analyzed for their colocalization to unveil if SYP is always co-expressed at SPO-positive synapses. In the CTX, PUT, and AMY, on average only around 4% of all SPO-positive puncta colocalized with SYP (Fig. 3a). In the region with the highest SPO expression, the HC, almost one fourth of SPO-positive synapses colocalized with SYP (Fig. 3b, 2). In the CB, more than half of the puncta colocalized (Fig. 3b, 8). The highest overlap between SYP and SPO was found in the SC DH with ~75% of total SPO puncta (Fig. 3b, 10). In the auditory system, around 57% of SPO-positive puncta did not colocalize with SYP in the IC (Fig. 3c, 4). In the SOC, roughly one third of all SPO-positive puncta did not colocalize (Fig. 3c, 3). In the region with the highest SPO and SYP expression, the MGB, the majority of the puncta colocalized (~21% SYP-negative; Fig. 3c, 5). The measured colocalization in the reference

[1] https://www.proteinatlas.org/ENSG00000163630-SYNPR/brain (accessed 22 February 2026)

region, the CTX, was in line with Fig. 3a.

Based on the high SPO RNA levels in the human putamen/striatum (Fig. S3d), we additionally analyzed globus pallidus and substantia nigra (SN) as target sites of striatal efferents (striatopallidal and striatonigral projections). In the globus pallidus (external segment), no SPO expression was observed (mean puncta density of 0.01; normalized to CTX; data not shown). In the SN tissue section, we found a striking pattern of intense SPO signal, mostly dorsal to the pars compacta of the SN (SNpc). The SPO signal was arranged like 'beads-on-a-string', most likely decorating a dendrite (Fig. S4a) with, on average, a twice as high puncta density when compared to the CTX (Fig. S4b) and a 2.5 times higher sum intensity (Fig. S4c). The putative dendrites showed a diverse pattern of synapses, with SPO and SYP single-positive synapses (Fig. S4d, top); on average 47% of all SPO puncta were SYP-positive (Fig. S4d, bottom). The exact anatomical localization of these intense SPO signals was confirmed in an entire tissue section from an additional case and via chromogen-based staining (Fig. S4e, note the localization of SPO in relation to the SNpc). Assuming that all dendrites of SN neurons stain for tyrosine hydroxylase, on average (case ID #2–4) only 24% of all SPO puncta were associated with SN dendrites in the described region (Fig. S4f, arrowheads).

2.5. Underestimation of synapse numbers in the human cerebral cortex with synaptophysin

Since the CTX is a relevant region to determine synapse density, we were surprised by the finding that 'pan-synaptic' SYP was not present at a considerable amount of SPO-positive synapses and, importantly, SPO was strongly expressed in the human CTX. We therefore aimed to validate our findings in additional human cerebral cortex tissue. In commercially available, paraffin-embedded tissue, we found a slightly lower, but still considerable amount of SPO+/SYP- puncta (Fig. 4a). Assuming that the sum of SPO+/SYP- and SYP-positive puncta reflects the total synapse number, SYP staining alone marked on average 'only' 81% of all synapses (i.e., loss of 19%). Similar results were obtained from immediately fixed and cryopreserved cortical tissues: First, in all additional cases, the majority of SPO-positive puncta was SYP-negative (Fig. 4b, Fig. S5a-b). Second, SYP staining alone consistently resulted in a loss of on average 27% of all synapses (Table S1). Overall, the additional cortical tissue confirmed the findings from the anatomy course brains (Fig. 1f), where SYP staining alone marked on average 'only' 86% of all synapses.

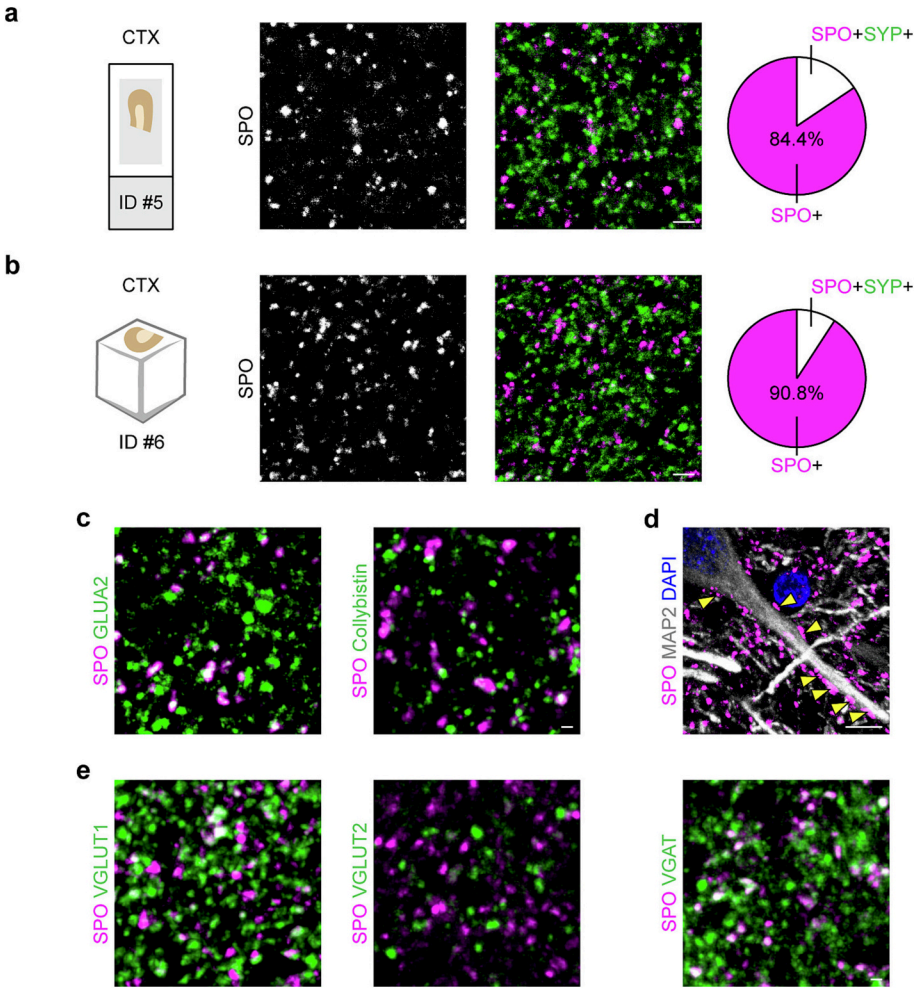

Fig. 4. Human cortical tissue from additional sources confirms low colocalization of SPO and SYP. Colocalization of SPO and SYP was analyzed in case ID #5 (a) and ID #6 (b) and is represented as pie chart (magenta = SPO+/SYP- surfaces, white = SPO+/SYP+ surfaces). Images represent MIPs of raw data. Scale bars: 3 µm. (c) Expression of SPO at excitatory (left) and inhibitory (right) synapses. Scale bar: 1 µm. (d) SPO is aligned along apical dendrites and around the soma of pyramidal neurons (yellow arrowheads). The image is presented in perspective view. Scale bar: 7 µm. (e) Verification of synaptic localization via pre-pre co-staining. Scale bar: 1 µm. A Gaussian filter with default filter width was applied to the raw images of panels (c) and (e), panels (c)-(e) show representative images of case ID #6. (For interpretation of the references to colour in this figure legend, the reader is referred to the web version of this article.)

2.6. SPO expression at excitatory and inhibitory synapses in the cerebral cortex

We finally aimed to determine the identity of SPO-positive synapses in the CTX. Since pre-post colocalizations are oftentimes used as criterion for mature synapse counting via IF, SPO co-staining with GLUA2 and collybistin was performed. In the body donors, on average 31% of SPO puncta were detected at GLUA2-positive excitatory synapses, in the cryopreserved tissue (ID #6), 49% of all puncta were associated with GLUA2 (Fig. 4c, left). In the same tissues, around 24% (37%) of SPO-positive puncta were located at collybistin-positive inhibitory synapses (Fig. 4c, right). In addition, co-staining with MAP2 showed that 80% of all SPO puncta were in close proximity to a dendrite. Interestingly, strong SPO signal was observed around cell somata and apical dendrites (Fig. 4d, on average six SPO puncta / 10 µm apical dendrite; average of seven neurons). To verify synaptic localization via pre-pre staining, SPO co-staining with VGLUT1, VGLUT2, and VGAT was performed in the cryopreserved tissue resectates (Fig. 4e, Table S1). While SPO was hardly found at VGLUT2-positive synapses, a clear overlap between SPO and VGAT was observed in all tissues. Apart from one case, a lower fraction of SPO puncta was found at VGLUT1-positive synapses (Table S1). In summary, SPO is not exclusively located at excitatory or inhibitory synapses.

Table 3
Comparison of human SPO RNA (The Human Protein Atlas) and protein levels.

Brain region[1]	RNA levels	Protein levels
HC	++	++
AMY	+	+
PUT	++	+
Pallidum	+	−
THA	+	−
MGB	+	+
IC	+	+
Pons	−	−
SO (RNA) / SOC (protein)	−	+
DCN (RNA) / CNC (protein)	+	−
IO	+	−
CB	++	+
SC VH	+	−
SC DH	+	++

++ higher than cortical levels, + moderate to low levels, − basically absent; for protein levels, the normalized SPO sum intensity was used as reference.
[1] hippocampus, CA3 (HC); lateral amygdala (AMY); putamen (PUT); globus pallidus, externus (pallidum); ventral thalamic nuclei (THA); medial geniculate body (MGB); inferior colliculus (IC); pontine nuclei (pons); superior olive (SO); superior olivary complex (SOC); dorsal cochlear nucleus (DCN); cochlear nuclear complex (CNC); inferior olive (IO); cerebellar cortex (CB); spinal cord, ventral horn (SC VH); spinal cord, dorsal horn (SC DH).

3. Discussion

In this study, synaptoporin (SPO), a presynaptic vesicle protein that has been significantly less studied than the family member synaptophysin (SYP), was found to be expressed not only in the human hippocampus (HC) but also in other subcortical (e.g., amygdala (AMY), putamen (PUT)) and cortical brain regions, as well as in the dorsal horn of the spinal cord (SC DH). Most important and contrary to our expectations, SPO was largely not detected at SYP-positive synapses. Since in the cerebral cortex (CTX), a region relevant for disease studies, SPO was expressed in considerable amounts, the experiments were repeated in human tissue from different sources. On average, SYP-only staining neglected at least up to 35% of the total amount of synapses.

Only little is known on the exact function of SPO. Initial studies hypothesize on a role during synaptic vesicle membrane fusion, eventually through the gap-junction like pores that arise from alpha-helices (Knaus et al., 1990; Ovtscharoff et al., 1993). Rodent studies imply a role of SPO after peripheral nerve injury, in particular for pain processing ((Chung et al., 2019), see also below). Second, an animal study on the mossy fiber-CA3 synapse suggests that SPO is relevant for mossy fiber upregulation after chronic inactivation of nerve impulses (Lee et al., 2013), pointing towards a possible link between SPO expression regulation and the treatment of seizures (Andre et al., 2018). In human studies, SPO has been frequently used as tool to highlight mossy fibers in tissue from epileptic patients (Freiman et al., 2021; Janz et al., 2017; Schmeiser et al., 2017) but detailed studies on its synaptic localization or function are lacking. The datasets in 'The Human Protein Atlas' (HPA) provide extensive RNA expression data but protein expression data are incomplete and not in a synapse-directed manner. In a study on the human HC, we could show previously that SPO is not only enriched in mossy fibers but also expressed in most of the hippocampal layers (Woelfle and Boeckers, 2021).

Apart from the HC, this study shows that SPO is present in considerable amounts in the human CTX, AMY, CB, and SC DH and with low levels in the PUT. In the rodent SC, SPO is also enriched in the dorsal horn (Chung et al., 2019; Sun et al., 2006). Detailed analysis of SPO-positive afferents in the SC was beyond the scope of this study but data from rodents suggest that SPO, but not SYP, is the dominant protein in both types (Aδ and C) of nociceptive fibers (Sun et al., 2006). Among all analyzed regions, the CB showed one of the largest variabilities between the cases. Interestingly, in the rat CB, in contrast to SYP, SPO is not expressed homogenously in the molecular layer but in a rostrocaudal gradient (Fykse et al., 1993). In future studies on the human CB, it would be interesting to explore whether this feature is conserved in humans and, if so, it might have contributed to the variable results on SPO expression in the present study. In general, the negative IF results from particular nuclei/layers of the THA, pons, and IO were in line with the data from the lysates of the entire brain region. For those regions, where lysates were available, the relative expression levels obtained by both methods (western blots and IF) were largely congruent. Overall, expression or absence of SPO is largely conserved in the human brain in comparison to rat (based on semi-quantitative RNA data from (Marqueze-Pouey et al., 1991)).

In Table 3, our protein expression data are compared to the available human RNA dataset (HPA, summarized in Fig. S3d). Relative expression levels of RNA and protein are not expected to match when neurons producing SPO RNA mainly project to other brain regions where the presynaptic SPO protein of these neurons can be found. Based on this principle, hypotheses on the cell type-specific expression of SPO can be formulated for regions with clearly diverging RNA and protein levels:

1) While SPO protein was absent from the entire medulla oblongata (−) and THA (−, see Table 3), RNA levels are almost in the magnitude of the AMY (+). This implies that neurons expressing SPO RNA in those regions project to other brain regions where they form synapses that contain the SPO protein. In particular, for the IO, SPO RNA might thus be expressed by glutamatergic neurons that give rise to climbing fibers. This is in line with the presence of SPO protein in the molecular layer of the CB.
2) For the cerebellar cortex, SPO RNA levels are higher than in the CTX (++), the protein levels are lower (+). This could indicate that the majority of SPO RNA is present in neurons that give rise to efferent fibers, i.e. Purkinje cells. Whether SPO is also expressed at parallel fibers was not studied in detail here but was concluded in a rodent study (Fykse et al., 1993).
3) A similar concept was proposed for the rodent striatum: high SPO RNA levels and low protein levels have led to the assumption that striatal efferents and few intrinsic or corticostriatal connections are SPO-positive and striatal afferents are mainly SYP-positive (Ovtscharoff et al., 1993). This trend is in line with the human RNA data (HPA, see Fig. S3d). To confirm the hypothesis on protein level, human substantia nigra (SN) and globus pallidus, the major target sites of striatal efferents, were stained for SPO. The globus

pallidus was devoid of SPO (−). Among the striking SPO signals dorsal to the human SN, only a very small fraction was aligned along tyrosine hydroxylase-positive SN dendrites. This could be explained by the fact that the majority of SN dendrites projects into the opposite direction, i.e., the pars reticulata (Braak and Braak, 1986). We do not securely know all types of dendrites that run along the SPO-intense region dorsal to the SN but our finding importantly shows that this region seems to be one of the brain regions with the highest densities of SPO-containing synapses; out of the studied regions even higher than in the HC and, thus, the highest density and the second highest expression level.

In summary, SPO is expressed in neocortical and allocortical brain regions that are involved in complex processes like learning, memory, emotion, movement control, and perception.

The human data from the auditory system largely match the protein expression in the mouse (Reuss et al., 2023). High to moderate SPO levels were found in the analyzed layers of the medial geniculate body (MGB; medial subdivision) and the IC (external CTX) and low to no expression was found in principal nuclei of the SOC and the cochlear nucleus complex (CNC; here: no specific analysis in the superficial layer of the dorsal nucleus). Remarkably, in humans and mice, SPO is hardly expressed in nuclei of the canonical auditory system (e.g., CNC and central nucleus of the IC (data not shown)) but rather in associated regions (Reuss et al., 2023).

Of particular interest is that SPO puncta were mostly not colocalized, i.e., on the same presynaptic terminal as SYP. This aspect has been marginally addressed in one of the initial studies via immunoprecipitation and IF in rodent tissue (Fykse et al., 1993). While a general overlap of SPO and SYP was reported, it has to be noted that immunoprecipitation was performed with whole brain lysates and the presence of some SPO+/SYP- synapses is discussed in the merely qualitative IF part. One major conclusion from the present study is, thus, that SYP is present at a large subset, but not at all synapses. A question that immediately arises from this finding is whether there is at all a presynaptic vesicle protein that is suited to label the majority, if not all, synapses. Reviewing the – mostly rodent – literature on the so-called brain synaptome hints towards a large diversity of synaptic subtypes. A very recent human study on the SV2A protein showed that only ~25% of all synapses in the temporal cortex are SV2A-positive and questioned the analysis in an initial study which, in their opinion, constitutes the cornerstone for the notion of SV2A as a suitable synaptic marker (Wong et al., 2025). This finding is of particular interest since SV2A has been a target for *in vivo* PET studies (Finnema et al., 2016). Besides, the example of SV2A underlines the necessity of high resolution quantitative studies in well characterized human tissue as a basis for clinical studies. In a large study on the combinatorial expression of synaptic proteins in the somatosensory cortex of transgenic mice, SYP and synapsin I as the only presynaptic vesicle proteins were identified at nearly every synapse. In direct comparison, synapsin I was suggested for immunohistochemical applications (Micheva et al., 2010). Yet, also with respect to other brain regions, literature has been cited which implies that synapsin I is not ubiquitous: A study in rat brains reported that only around 33% of all VGAT-positive synapses are synapsin I-positive, 45% are SYP-positive (Bragina et al., 2007); which is contraintuitive to the definition of a 'pan-synaptic' marker. The variability of synaptic subtypes defined by the presence or absence of synaptic vesicle proteins is not surprising. A comprehensive study on the mouse synaptome found the same when studying PSD95/SAP102 combinatorial expression (Zhu et al., 2018). Two intriguing studies (Bulovaite et al., 2022; Cizeron et al., 2020) unveiled the dynamics of these synapses during aging and the diverging protein lifetimes in health and disease in a mouse model which further adds complexity on the understanding of the variable synaptic subtypes. Taken together, the presence of a true 'pan-synaptic' marker is unlikely. For IHC, a suited approach might be the combination of two markers like SYP and SPO or SYP and synapsin I to capture the majority of synapses.

The majority of SPO could be assigned to inhibitory or excitatory synapses. When reviewing the data (Table S1), it seems conceivable that for both combinations (pre-pre and pre-post), some SPO puncta are not colocalized with either of the applied excitatory or inhibitory marker protein. The plausible reasons for this are manifold: SPO might be expressed at cholinergic and/or monoaminergic terminals of the CTX (Peter et al., 1995; Weihe et al., 1996). Another possibility is that these synapses define a so far undescribed group of synapses. Interestingly, a very recent study identified VGLUT1- and Gephyrin-positive synaptic sites; albeit their functional contribution remains to be unveiled (Unterauer et al., 2024). Besides, the applied antibodies are known to label the majority of excitatory or inhibitory synapses but recent research undermines the combinatorial complexity: For collybistin, variable expression levels at inhibitory synapses were reported (Patrizi et al., 2012). In addition, we observed several SPO-positive puncta around the somata and apical dendrites of pyramidal neurons. A recent study (Kuljis et al., 2021) found that a considerable fraction of these inhibitory synapses (Alonso-Nanclares et al., 2004) are gephyrin-negative (and therefore, most likely, also collybistin-negative). Taken together, based on single cell RNA data from 'The HPA',[2] SPO is mainly located in neurons, making a substantial glial contribution to cortical SPO expression unlikely. In line with this, most of the SPO puncta were aligned along dendrites, which confirms synaptic localization. Overall, our findings are in support of the concept of a highly diverse synaptome.

In summary, this study provides detailed expression data on the presynaptic vesicle protein synaptoporin in the human brain. SPO has been mainly neglected so far but co-staining of SYP and SPO in the CTX, a region with high SPO levels, shows the presence of a considerable number of SPO+/SYP- synapses. This finding is relevant in the context of identifying disease-prone subtypes (e.g., (Marcassa et al., 2025)) and studies of this kind are needed to identify targets for suitable PET tracers in the clinics. Developments in the usually destructive biochemical methods partially keep the spatial aspect when identifying synaptic subtypes (e.g., (Biesemann et al., 2014) and (van Oostrum et al., 2023)) but they require rodent models. Overall, the magnitude of synaptic subtypes should be addressed in greater detail in future human studies to identify disease-prone subtypes.

4. Methods

4.1. Western blot analysis of human tissue lysates

The following human brain tissue lysates (tissue type: normal) were purchased from GeneTex; based on the delivered LOT, the company kindly provided information on the donors: cerebral cortex (GTX28736; male, 78 years), amygdala (GTX28766; male, 22 years), hippocampus (GTX28726; male, 71 years), thalamus (GTX28710; male, 75 years), diencephalon (GTX28729; male, 66 years), medulla oblongata (GTX28721; female, 60 years), pons (GTX28714; male, 66 years), and cerebellum right (GTX15357; male, 66 years). A protein ladder (Spectra Multicolor Broad Range, Thermo Scientific) and 20 μg of each lysate were separated on 4–15% stain-free TGX precast gels (Bio-Rad). To distinguish synaptophysin I (SYP) and synaptoporin (SPO) on the same membrane, the membrane was first incubated with the SPO antibody (1:1000, Cat# 102003, RRID:AB_2619748, Synaptic Systems) and the signal was visualized with the Clarity western ECL Substrate kit (Bio-Rad). Afterwards, the membrane was incubated with the SYP antibody (1:1000, Cat# 101004, RRID:AB_1210382, Synaptic Systems) and the signal was visualized via immunofluorescence (Alexa Fluor donkey anti-guinea pig, 1:1000, Jackson ImmunoResearch Laboratories, Inc.) at a ChemiDoc MP Imaging System (Bio-Rad). Signal intensities from the respective antibodies were normalized to the total protein stain using

[2] https://www.proteinatlas.org/ENSG00000163630-SYNPR/single+cell (accessed 22 February 2026)

the Image Lab software (vers. 6.1.0.07, Bio-Rad) and then normalized to the cerebral cortex. The mean of two replicates was plotted in GraphPad Prism 6 (vers. 6.07, GraphPad software).

4.2. Post mortem human brain tissue

Post mortem human brain tissue was derived from permanent body donors of the gross anatomy course (Institute for Anatomy and Cell Biology, Ulm University). A positive ethics vote had been obtained (ethics committee of Ulm University). Following the anatomy course, brains were immersion-fixed in 1% phosphate-buffered formaldehyde. For full information on the fixation procedure, see (Woelfle et al., 2023a). Details on the included cases can be found in Table 1, case ID #1–4. Tissue blocks were excised from the left hemisphere and further processed with a vibratome (Microm HM 650 V, Thermo Scientific or VT1200S vibratome, Leica) to obtain 60 µm thick sections for immunofluorescence staining and Nissl staining. The latter were stored in 1× Dulbecco's phosphate-buffered saline (DPBS, Thermo Fisher Scientific) + 0.02% sodium azide (Carl Roth) at 4 °C. Cerebral cortex tissue slides (tissue type: normal, 5 µm thick sections) were obtained from GeneTex (GTX24296) (Table 1, case ID #5). In addition, tissue from an immediately fixed, cryopreserved part from the human temporal pole (see epilepsy patient in (Woelfle et al., 2023b), Table 1, case ID #6) and tissue resectates (cortical access tissue) from brain surgery (Table 1, case ID #7 and ID #8) was used in this study. For the latter, tissue was fixed overnight in 4% PFA in PBS, pH 7.4 (Morphisto) and kept in 30% sucrose in 1× DPBS for 72 h. Finally, tissue was embedded in Tissue-Tek O.C.T. compound (Sakura) and stored at −80 °C. For all cryopreserved tissues, 40 µm thick sections for immunofluorescence staining were cut on a cryostat (Leica CM3050 S cryostat). The patients had provided their written and informed consent for participation in the studies. The studies were approved by the ethics committee of Ulm University and Cottbus.

4.3. Immunofluorescence staining of post mortem human brain tissue

Immunofluorescence staining was performed as previously described (Woelfle and Boeckers, 2021). The primary antibodies were diluted 1:200 (SPO) and 1:500 (SYP) in blocking solution. The following additional antibodies were used: collybistin-mouse (1:80, Cat# MAB7848, RRID:AB_3658942, R and D Systems), VGAT-mouse (1:80, Cat# 131011, RRID:AB_887872, Synaptic Systems), GLUA2-mouse (1:200, Cat# 182111, RRID:AB_10645888, Synaptic Systems), VGLUT1-gp (1:200, Cat# 135318, RRID:AB_2924948, Synaptic Systems), VGLUT2-mouse (1:100, Cat# MAB5504, RRID:AB_2187552, Millipore), MAP2-chicken (1:2000, Cat# CPCA-MAP2, RRID:AB_2138173, EnCor Biotechnology), and tyrosine hydroxylase-mouse (TH, 1:200, Cat# MAB318, RRID:AB_2201528, Millipore). For most antibodies (VGAT, GLUA2, VGLUT1, VGLUT2, and TH), heat-induced epitope retrieval (HIER) was performed: tissue sections were boiled in 0.1 M citrate buffer (pH 6) for 20 min in a water bath. Alexa Fluor 647-, 594- (MAP2), 488-, (Jackson ImmunoResearch Laboratories, Inc.), STAR GREEN-, and STAR RED- and STAR ORANGE-conjugated (Abberior, the last pair only for TH/SPO co-staining) secondary antibodies were used at a dilution of 1:200.

GeneTex tissue slides were deparaffinized in xylene and hydrated in a decreasing alcohol series. Blocking took place for 2 h, primary antibody incubation time was overnight at 4 °C. Washing times before and after secondary antibody incubation (2 h) were reduced to 3× 30 min, each. DAPI was applied at 1:50,000 in 1× DPBS. The cryopreserved tissue was stored in cryoprotectant solution at −20 °C and washed three times in 1× DPBS before immunostaining. In each staining round, negative controls (i.e., no primary antibody) were included and yielded no staining apart from autofluorescent lipofuscin (Fig. S6).

Figs. 1 & 4: Images were acquired using the 40× oil objective (ACS Apo; numerical aperture (NA) 1.15; free working distance (WD) 270 µm) at a SPE confocal laser-scanning microscope (Leica) with the camera set to 12 bit. *Z*-stacks with z = 1.98 µm were acquired at 0.22 µm intervals. Fig. 2: Images were acquired using a 40× oil objective (Iris 440756; NA 1.0) and the confocal mode of a STEDYCON system (Abberior). Z-stacks with z = 2 µm were acquired at 0.2 µm intervals.

4.4. Chromogen-based staining of post mortem human brain tissue

Alzheimer's disease (AD) staging and Parkinson's disease (PD) staging was performed as previously described (Woelfle and Boeckers, 2021).

Tissue sections were briefly rinsed in 1× DPBS. If not stated differently, all incubation steps were performed at room temperature under gentle agitation. Endogenous peroxidase was blocked with 3% H_2O_2 in 1× DPBS for at least 30 min (or until no bubbles were observed anymore). After 3 rinses à 3 min, tissue sections were blocked for 90 min (5% BSA in 1× DPBS plus 0.25% Triton X-100). The SPO antibody was diluted 1:200 in 1× DPBS and incubated with the tissue sections overnight at 4 °C. On the next day, tissue sections were washed 3× 3 min in 1× DPBS and the biotinylated goat anti-rabbit secondary antibody (Cat# BA-1000, RRID:AB_2313606, Vector Laboratories) was diluted 1:200 in 1× DPBS and applied for 90 min. Afterwards, tissues sections were washed 3× 3 min in 1× DPBS and the previously (at least 30 min before usage) prepared ABC mix (Vectastain Elite ABC Kit, Peroxidase (Standard), PK-6100, Vector Laboratories) was added to the tissue sections for 2 h. Tissue sections were washed 3× 3 min in 1× DPBS before the chromogen was applied. For a better contrast to the substantia nigra, a blue chromogen (VEC-SK-4700, Vector Laboratories) was used following the manufacturer's instructions; negative controls without primary or secondary antibody were performed. Finally, tissue sections were placed on filter paper in 70% isopropanol and dehydrated (96% isopropanol and 2× 100% isopropanol, each step 20 min or last incubation overnight). After incubation in xylene (2×, short), tissue sections were mounted in Eukitt (Sigma-Aldrich) and coverslipped.

An overview scan was acquired in brightfield mode with a colour camera and with the 4× dry objective (Plan Apochromat; NA 0.2; WD 20 mm) of a Biorevo BZ-X810 microscope (Keyence), a subregion of the tissue section was acquired with a 20× dry objective (Plan Apochromat; NA 0.75; WD 0.6 mm).

4.5. Nissl staining of post mortem human brain tissue

Human tissue sections were briefly rinsed in Milli-Q water and stained for 1–5 min in 0.5% aqueous cresyl violet (Carl Roth) solution supplemented by a few drops of 10% acetic acid glacial (VWR). Tissue sections were differentiated and dehydrated in 96% ethanol, further dehydrated in 100% isopropanol (2× à 20 min or second incubation overnight), incubated in xylene (2×, short) and mounted in Eukitt mounting medium.

Images of entire tissue sections were obtained with a Biorevo BZ-X810 microscope (Keyence) as described elsewhere (Woelfle and Boeckers, 2021).

4.6. Image analysis

First, images were deconvolved in Huygens software (vers. 24.10, Scientific Volume Imaging) to increase signal to noise ratio.

Second, deconvolved images were opened with the 3D software Imaris (Imaris 10, Oxford Instruments). In the 3D z-stacks, immunostained structures were detected as ‘Surfaces’ using manually defined creation parameters. For comparing brain regions, per staining round, creation parameters for each channel were kept constant. Analysis was performed in three regions of interest (ROIs) per image; the DAPI signal was activated to place the ROIs in the neuropil. The sums for the parameters ‘surface number’ and ‘sum intensity’ were exported (Imaris statistics tab, ‘detailed’) from each ROI and added up (result: number

and sum intensity of all detected surfaces in the three ROIs). In this way, three images per brain region were analyzed. Finally, for both parameters, the mean of the three images was calculated, normalized to the cerebral cortex, and plotted. Exceptions: For the HC (SPO), and the SC VH and DH (SYP), automatically detected surfaces were manually unified since most likely due to the complex shape, one single surface was heavily segmented by the software (Fig. 1). For Fig. 4 & Table S1, two tissue sections were analyzed and the mean of ten (ID #5) and six regions of interest (ID #6–8) was calculated.

Controls: No surfaces were detected in the negative controls which were analyzed with the same parameters as the actual staining.

Colocalization: 1) Pre-pre: A surface was counted as colocalized when the overlapped volume ratio of a SPO-positive surface was 0.3 or higher. In other words, when 30% or more of the volume of a SPO-positive surface were covered by the second presynaptic protein, it was counted as colocalized surface. 2) Pre-post: To determine if presynaptic SPO and a postsynaptic protein are located at the same synapse, surfaces were transformed to spots and the 'colocalize spots' tool was used (Fogarty et al., 2013).

Dendritic localization: Surfaces were transformed to spots and filtered for those spots with a distance of <1 μm to a MAP2-positive dendrite (see also (Fogarty et al., 2013)).

If not stated differently in the figure legends, all confocal images shown within this article represent maximum intensity projections of raw data, but, importantly, analysis was performed on non-projected 3D stacks in Imaris as outlined above.

Supplementary data to this article can be found online at https://doi.org/10.1016/j.nbd.2026.107503.

CRediT authorship contribution statement

Sarah Woelfle: Writing – original draft, Visualization, Supervision, Methodology, Investigation, Funding acquisition, Formal analysis, Conceptualization, Writing – review & editing. **Michael Schön:** Resources, Investigation. **Maria T. Pedro:** Resources. **Jan Wagner:** Resources. **Ehab Shiban:** Resources. **Bujung Hong:** Resources. **Yuriy Tsoy:** Resources. **Tobias M. Boeckers:** Writing – review & editing, Resources, Funding acquisition.

Consent for publication

Not applicable.

Ethics approval and consent to participate

This study was approved by the ethics committee of Ulm University, Ulm and Cottbus. Informed consent was obtained for all cases.

Funding

SW is supported by the Bausteinprogramm of the Medical Faculty (Ulm University). The project was furthermore supported by the DFG, CRC1506 (Aging, A01) to TMB.

Declaration of competing interest

The authors declare that they have no known competing financial interests or personal relationships that could have appeared to influence the work reported in this paper.

Acknowledgements

Most important, our thanks go to the permanent body donors of the Institute for Anatomy and Cell Biology for making such studies possible and the patients for participation in the study. Besides, we thank Fatih Gültekin for technical support, Katharina Mangus and Simone Feldengut for technical support with AD/PD staging, and Kornelia Knetsch (study nurse).

Data availability

Data not included into the manuscript may be released upon reasonable request to the corresponding authors and in compliance with the ethics votes.

References

Alonso-Nanclares, L., et al., 2004. Synaptology of the proximal segment of pyramidal cell basal dendrites. Eur. J. Neurosci. 19, 771–776.
Andre, E.A., et al., 2018. What goes up must come down: homeostatic synaptic plasticity strategies in neurological disease. Future Neurol. 13, 13–21.
Bergmann, M., et al., 1993. Synaptophysin and synaptoporin expression in the developing rat olfactory system. Brain Res. Dev. Brain Res. 74, 235–244.
Biesemann, C., et al., 2014. Proteomic screening of glutamatergic mouse brain synaptosomes isolated by fluorescence activated sorting. EMBO J. 33, 157–170.
Braak, H., Braak, E., 1986. Nuclear configuration and neuronal types of the nucleus Niger in the brain of the human adult. Hum. Neurobiol. 5, 71–82.
Bragina, L., et al., 2007. Heterogeneity of glutamatergic and GABAergic release machinery in cerebral cortex. Neuroscience 146, 1829–1840.
Bulovaite, E., et al., 2022. A brain atlas of synapse protein lifetime across the mouse lifespan. Neuron 110, 4057–4073 e8.
Casseday, J.H., Schreiner, Christoph E., Winer, Jeffery A., 2005. The inferior colliculus: Past, present, and future. In: Winer, J.A., Schreiner, Christoph E. (Eds.), The Inferior Colliculus. Springer, pp. 626–640.
Chung, J., et al., 2019. Central expression of synaptophysin and synaptoporin in nociceptive afferent subtypes in the dorsal horn. Sci. Rep. 9, 4273.
Cizeron, M., et al., 2020. A brainwide atlas of synapses across the mouse life span. Science 369, 270–275.
DeKosky, S.T., Scheff, S.W., 1990. Synapse loss in frontal cortex biopsies in Alzheimer's disease: correlation with cognitive severity. Ann. Neurol. 27, 457–464.
Finnema, S.J., et al., 2016. Imaging synaptic density in the living human brain. Sci. Transl. Med. 8, 348ra96.
Fogarty, M.J., et al., 2013. A method for the three-dimensional reconstruction of Neurobiotin-filled neurons and the location of their synaptic inputs. Front. Neural Circuits 7, 153.
Freiman, T.M., et al., 2021. Mossy fiber sprouting into the hippocampal region CA2 in patients with temporal lobe epilepsy. Hippocampus 31, 580–592.
Fykse, E.M., et al., 1993. Relative properties and localizations of synaptic vesicle protein isoforms: the case of the synaptophysins. J. Neurosci. 13, 4997–5007.
Grabs, D., et al., 1994. Differential expression of synaptophysin and synaptoporin during pre- and postnatal development of the rat hippocampal network. Eur. J. Neurosci. 6, 1765–1771.
Jahn, R., et al., 1985. A 38,000-Dalton membrane protein (p38) present in synaptic vesicles. Proc. Natl. Acad. Sci. USA 82, 4137–4141.
Janz, P., et al., 2017. Early tissue damage and microstructural reorganization predict disease severity in experimental epilepsy. Elife 6, e25742.
Knaus, P., et al., 1990. Synaptoporin, a novel putative channel protein of synaptic vesicles. Neuron 5, 453–462.
Kuljis, D.A., et al., 2021. Gephyrin-lacking PV synapses on neocortical pyramidal neurons. Int. J. Mol. Sci. 22.
Lavezzi, A.M., Matturri, L., 2012. Neuroanatomical dysmorphology of the medial superior olivary nucleus in sudden fetal and infant death. Front. Hum. Neurosci. 6, 322.
Lee, K.J., et al., 2013. Mossy fiber-CA3 synapses mediate homeostatic plasticity in mature hippocampal neurons. Neuron 77, 99–114.
Leube, R.E., et al., 1987. Synaptophysin: molecular organization and mRNA expression as determined from cloned cDNA. EMBO J. 6, 3261–3268.
Mansour, Y., et al., 2019. Characterization of the human central nucleus of the inferior colliculus. Hear. Res. 377, 234–246.
Marcassa, G., et al., 2025. Synaptic signatures and disease vulnerabilities of layer 5 pyramidal neurons. Nat. Commun. 16, 228.
Marqueze-Pouey, B., et al., 1991. Differential expression of synaptophysin and synaptoporin mRNAs in the postnatal rat central nervous system. J. Neurosci. 11, 3388–3397.
Micheva, K.D., et al., 2010. Single-synapse analysis of a diverse synapse population: proteomic imaging methods and markers. Neuron 68, 639–653.
Ovtscharoff, W., et al., 1993. Ontogeny of synaptophysin and synaptoporin in the central nervous system: differential expression in striatal neurons and their afferents during development. Brain Res. Dev. Brain Res. 72, 219–225.
Pal, I., et al., 2019. Morphological and neurochemical changes in GABAergic neurons of the aging human inferior colliculus. Hear. Res. 377, 318–329.
Patrizi, A., et al., 2012. Selective localization of collybistin at a subset of inhibitory synapses in brain circuits. J. Comp. Neurol. 520, 130–141.
Peter, D., et al., 1995. Differential expression of two vesicular monoamine transporters. J. Neurosci. 15, 6179–6188.
Reuss, S., et al., 2023. Synaptoporin and parathyroid hormone 2 as markers of multimodal inputs to the auditory brainstem. J. Chem. Neuroanat. 130, 102259.
Scheff, S.W., et al., 1990. Quantitative assessment of cortical synaptic density in Alzheimer's disease. Neurobiol. Aging 11, 29–37.

Scheff, S.W., et al., 2006. Hippocampal synaptic loss in early Alzheimer's disease and mild cognitive impairment. Neurobiol. Aging 27, 1372–1384.
Schmeiser, B., et al., 2017. Extent of mossy fiber sprouting in patients with mesiotemporal lobe epilepsy correlates with neuronal cell loss and granule cell dispersion. Epilepsy Res. 129, 51–58.
Siew, L.K., et al., 2004. Measurement of pre- and post-synaptic proteins in cerebral cortex: effects of post-mortem delay. J. Neurosci. Methods 139, 153–159.
Singec, I., et al., 2002. Synaptic vesicle protein synaptoporin is differently expressed by subpopulations of mouse hippocampal neurons. J. Comp. Neurol. 452, 139–153.
Sitek, K.R., et al., 2022. Structural connectivity of human inferior colliculus subdivisions using in vivo and post mortem diffusion MRI Tractography. Front. Neurosci. 16, 751595.
Sun, T., et al., 2006. Differential expression of synaptoporin and synaptophysin in primary sensory neurons and up-regulation of synaptoporin after peripheral nerve injury. Neuroscience 141, 1233–1245.
Tardif, E., et al., 2003. Patterns of calcium-binding proteins in human inferior colliculus: identification of subdivisions and evidence for putative parallel systems. Neuroscience 116, 1111–1121.
Unterauer, E.M., et al., 2024. Spatial proteomics in neurons at single-protein resolution. Cell 187, 1785–1800 e16.
van Oostrum, M., Schuman, E.M., 2025. Understanding the molecular diversity of synapses. Nat. Rev. Neurosci. 26, 65–81.
van Oostrum, M., et al., 2023. The proteomic landscape of synaptic diversity across brain regions and cell types. Cell 186, 5411–5427 e23.
Weihe, E., et al., 1996. Visualization of the vesicular acetylcholine transporter in cholinergic nerve terminals and its targeting to a specific population of small synaptic vesicles. Proc. Natl. Acad. Sci. USA 93, 3547–3552.
Wiedenmann, B., Franke, W.W., 1985. Identification and localization of synaptophysin, an integral membrane glycoprotein of Mr 38,000 characteristic of presynaptic vesicles. Cell 41, 1017–1028.
Woelfle, S., Boeckers, T.M., 2021. Layer-specific vesicular glutamate transporter 1 immunofluorescence levels delineate all layers of the human Hippocampus including the stratum lucidum. Front. Cell. Neurosci. 15, 789903.
Woelfle, S., et al., 2023a. CLARITY increases sensitivity and specificity of fluorescence immunostaining in long-term archived human brain tissue. BMC Biol. 21, 113.
Woelfle, S., et al., 2023b. Expression profiles of the autism-related SHANK proteins in the human brain. BMC Biol. 21, 254.
Wong, T., et al., 2025. SV2A is expressed in synapse subpopulations in mouse and human brain: implications for PET radiotracer studies. Wellcome Open Res. 10, 415.
Zhu, F., et al., 2018. Architecture of the mouse brain synaptome. Neuron 99, 781–799 e10.